

# Crystal asymmetry induces single-atom chain formation in gold nanowires

Francesca Tavazza<sup>1</sup>, Anwar Hasmy<sup>2,3</sup>, Lyle E. Levine<sup>1</sup>, Anne M.

Chaka<sup>1</sup>, Luis Rincón<sup>2,4</sup>, M. Márquez<sup>2,5</sup> and Carlos González<sup>2</sup>

<sup>1</sup>National Institute of Standards and Technology, Gaithersburg, MD 20899, USA

<sup>2</sup>NIST Center for Theoretical and Computational Nanosciences, Gaithersburg, MD 20899, USA

<sup>3</sup>INEST Group Postgraduate Program, Philip Morris USA, Richmond, VA 23234, USA

<sup>4</sup>Departamento de Química, Universidad de los Andes, Mérida-5101, Venezuela and

<sup>5</sup>Research Center, Philip Morris USA, Richmond, VA 23234, USA

(Dated: July 7, 2019)

We performed density functional theory and tight-binding molecular dynamics calculations to investigate the formation of suspended linear atom chains when stretching gold nanowires along the [110] crystal orientation. We determined that chain formation can occur only when the crystal symmetry is broken in the early stages of the elongation process. Such crystallographic asymmetry can be induced by stretching the wire along a slightly off-axis tensile direction or by introducing thermal fluctuations. Our observation of the off-axis formation of these chains agrees with experimental findings.

PACS numbers: 61.46.-w, 73.63.Bd, 68.65.-k, 62.25.+g

Nanowires (NWs) exhibit interesting properties that may be exploited to generate novel electronic devices[1]. One of the most exciting properties is the observed high stability of suspended single-atom chains (SACs) that form during the stretching of gold NWs[2, 3, 4, 5, 6]. The formation of SACs also suggests that gold NWs may be useful as an intrinsic force standard. However, little is known about the geometrical conditions required for such single-atom chain formation. In particular, conflicting experimental results have been reported for NWs elongated along the [110] high-symmetry axis[4, 5, 6]. From the theoretical point of view, density functional theory (DFT) calculations have failed to describe the formation of SACs[7, 8]. Due to the high computational cost, none of these numerical efforts described the dynamics of the chain formation under strain. Other studies have considered molecular dynamics simulations of gold SACs based on classical many-body empirical potentials[9, 10, 11, 12, 13, 14]. Although they provided useful insights into the SAC formation process, classical approximations are unreliable when quantum effects become relevant, and predictions of [110] SAC formation depends upon the specific classical potential used[9, 10, 12]. Da Silva *et al.*[15, 16] combined a description of the electronic structure and the dynamics of the breaking process by using tight-binding molecular dynamics (TBMD) simulations. The probability of linear single-atom chain formation, as well the number of atoms within the chains, match the experimental observations[16]. Their work, however, only focused on the dynamics of chain formation along the [111] crystallographic orientation.

In this letter we address the “[110] controversy,” by performing semistatic quantum relaxation calculations using DFT for a first principles description of the underlying energy landscape and the low-energy atomic configurations, and molecular dynamics simulations within the NRL-Tight Binding approximation[17] to describe the dynamics effects within the system during deformation.

To investigate the breaking mechanism of [110]-oriented NWs stretched along a [110] tensile axis, we considered both the ideal case, where the tensile axis is perfectly aligned along the [110] crystallographic direction, and a more realistic one, where the crystal symmetry is broken either by applying the strain slightly off-axis or by introducing thermal fluctuations.

The DFT calculations were performed using DMol<sup>3</sup>[18, 19, 20]. In DMol<sup>3</sup>, the physical wave function is expanded in a numerical basis set, and fast convergent three-dimensional integration is used to calculate the matrix elements occurring in the Ritz variational method. We used a real-space cutoff of 0.4 nm and a double-zeta, atom-centered basis set (dnd). We utilized a generalized gradient approximation (GGA) approach (Perdew-Burke-Ernzerhof[21]), and a hardness conserving semilocal pseudopotential (dspp[22], only electrons with  $n=5$  and  $n=6$  were handled explicitly). The geometry optimization was performed using a conjugate gradient approach based on a delocalized internal coordinate scheme[23, 24]. In our DFT calculations we considered NWs with an axis parallel to a [110] crystallographic orientation and, initially, atoms in their bulk positions. Three combinations of tensile axes were used: [110], [99 101 2] (about 1° off the [110]), and [110] followed by [99 101 2]. Our simulation cell contained 115 atoms and, to eliminate self-interactions between the ends of the chain, a cluster configuration was used. Initially, the central part of the NW contained 9 alternating planes with 4 or 5 atoms each (see Fig. 1). Two atomic layers at the top and bottom served as grips and both single and double sided stretching modes were used. The grip atoms were incrementally moved along the tensile ( $z$ ) axis by  $\Delta z = 0.029$  nm for the [110] case and along  $\Delta x=0.00029$  nm,  $\Delta y=0.00058$  nm and  $\Delta z=0.029$  nm for the [99 101 2] case. After each tensile increment, the grip atoms were kept fixed while all of the other atoms were allowed to relax into new configurations. Usually, the system was

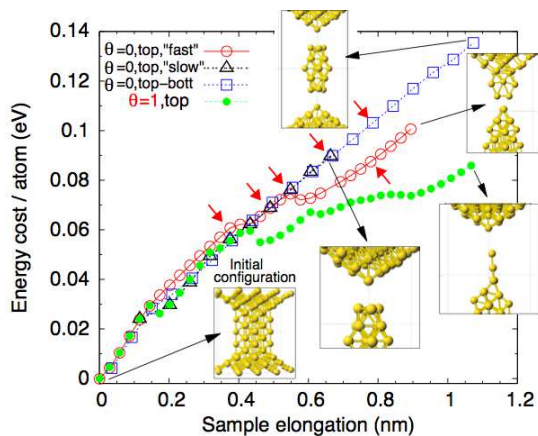


FIG. 1: Energy cost per atom versus sample elongation for selected simulations. Deformation along the  $[110]$  and  $[99\ 101\ 2]$  tensile axes is labeled “ $\theta = 0$ ” and “ $\theta = 1$ ”, respectively. The notation “top” indicates that the NW was stretched from one end only, while “top-bott” indicates symmetrical stretching. Examples of final configurations are displayed. The small arrows indicate  $[110]$  tensile axis configurations later used as starting points for  $[99\ 101\ 2]$  tensile axis simulations.

considered converged when the change in total energy per atom was less than  $5 \times 10^{-6}$  eV and changes in the gradient of the free atomic positions were less than  $3 \times 10^{-4}$  eV/Å. This methodology has been extensively used in recent years when studying nanowire deformation[25]. Different effective strain rates were simulated by slightly changing the convergence criteria on the gradient of the atomic positions, similar to the procedure in Picaud *et al.*[26].

The DFT results indicate that initially perfect NWs always break abruptly (i.e. simultaneously breaking more than one bond) when stretched along the  $[110]$  axis, in agreement with the observations of Rodrigues *et al.*[5]. This behavior is caused by the high symmetry of the system where all preferred slip directions are identical and the system cannot choose one over the other. Abrupt breaking is found for all effective strain rates and stretching modes, even though the energy path and atomic configurations depend on those quantities, indicative of a relatively flat yet complex energy surface. As a general rule, we find that there is less atomic rearrangement at lower effective strain rates. Also, abrupt breaking has a higher energy cost than SAC formation. These results are illustrated in Fig. 1, where the energy cost per atom versus elongation, and the corresponding final structures, are displayed for our most representative simulations. Calculations performed using the  $[110]$  tensile axis are indicated by  $\theta=0$ . Initially, the NW deforms elastically, and the energy path is identical in all cases. In the plastic regime, comparing only the simulations with single-sided stretching (open circles and triangles), we see that the larger atomic rearrangements at higher effective strain rates (open circles) result in larger final elongations ( $\approx 0.9$  nm compared to  $\approx 0.7$  nm) and higher energies.

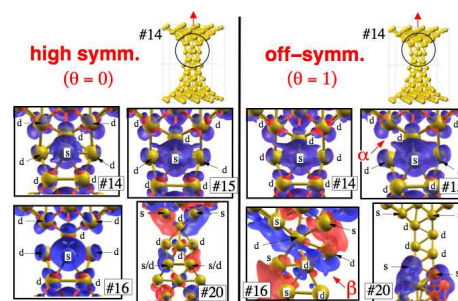


FIG. 2: Atomic arrangements and HOMO isosurfaces for crucial steps (14, 15, 16, 20) in the evolution of the NW for tensile axes  $[110]$  ( $\theta=0$ ) and  $[99\ 101\ 2]$  ( $\theta=1$ ). For each atom, the prevailing orbital character is specified (positive and negative lobes are colored blue and red, respectively).

The final force necessary to break a NW pulled along the  $[110]$  crystallographic direction is very consistent and independent of the strain rate and stretching mechanism: the average of all our simulations is  $-2.17$  nN $\pm 0.03$  nN. Figure 1 also shows results from the slightly off-symmetry  $[99\ 101\ 2]$  tensile axis (solid circles,  $\theta=1$ ). Here, the NW evolves basically identically to the high symmetry case for elongations up to 0.4 nm. For larger strains, significantly lower energy configurations are found, resulting in the formation of a SAC, which has also been observed experimentally[6].

Details of the atomic evolution of the NW and a direct comparison with the high symmetry case are displayed in Figure 2. Here, the off-axis geometry produces classic positive and negative stress concentration points at the base of the NW. Up to the 14th elongation step, the asymmetric stresses are too small to produce any significant differences between the two cases. In the 15th step, the stresses at the base of the NW produce an asymmetric bond failure (see arrow  $\alpha$ ) that drastically changes the stress distribution and produces further asymmetric bond breaking events in subsequent steps (see arrow  $\beta$ , step 16). The asymmetric deformation of the chain also significantly affects the electronic structure of the NW. While the highest occupied molecular orbitals (HOMO) are almost identical in the two cases up to the 13th step, they start differing in the 14th at the incipient failure point labeled  $\alpha$  in the 15th step. In the 15th step, the large  $s$  orbital of the central atom is now markedly asymmetric and electronic configurations are completely different from one another from the 16th step on. In the 16th elongation step, the HOMOs are still very localized on each atomic site in the high symmetry case, while the off-symmetry configuration shows more interatomic  $d$ -orbital bonding, especially along the  $\{111\}$  planes. Lastly, for strains larger than 33% (steps 20 and higher), the off-axis case displays a noticeable reduction in the HOMO states along the thinned out part of the NW. For this geometry, conventional slip on  $\{111\}$  planes is not observed; instead, thinning occurs through a progressive “unzipping” process. The energy

cost for a given strain increment is much lower for the off-symmetry case (Figure 1) because less energy is stored elastically. As shown in Fig. 1, a higher engineering strain is found for the off-symmetry case (0.61) than for the high-symmetry one (at most 0.52), when comparing runs with the same stretching mechanism. The force needed to break the NW is lower for the slightly off-symmetry case ( $-1.53 \text{ nN} \pm 0.02 \text{ nN}$ , a value close to that reported in experiments[11]), which is consistent with the breaking of just one bond instead of at least two, as occurred for the  $\theta=0$  case.

The above results suggest that abrupt (multi-bond) breaking is an unstable process and that small perturbations away from the symmetric case allow lower-energy atomic configurations to be reached, leading ultimately to SAC formation. To test this, we investigated the stability of intermediate structures by straining initially along the [110] axis and then shifting the tensile axis to [99 101 2]. The small arrows in Fig. 1 indicate the configurations that were used as starting points for the new  $\theta=1$  simulations (whose energetics are not shown in the figure). Surprisingly, the symmetric deformation path is quite stable. We observed SAC formation in only 2 cases, both of them when starting from simulations where a relatively high degree of atomic reorganization had occurred, and only using a relatively high effective strain rate. In both cases, the SAC was very short, only two atoms. All of the other dual-path simulations ended in abrupt breaking. These findings suggest that atomic configurations can be reached that are metastable. If perturbations are small enough, then abrupt breaking can occur. Below we will discuss this further, with respect to thermal fluctuations. Lastly, we performed similar calculations for a [111] NW elongated along the [111] tensile axis. In this case, we found SAC formation in both the perfectly symmetric and the slightly off-symmetry cases. We conclude that, from a thermodynamic stand point, there is an intrinsic difference in the evolution path of stretched gold NWs, depending on the crystallographic direction ([110] or [111]) of the tensile axis.

To evaluate the impact of kinetics on the morphology and evolution of the wire, we performed MD simulations of the wire under stress using the TBINS code[27], which is based on a TB approximation within the parameterization scheme proposed by Mehl and Papaconstantopoulos[17]. In this approximation, the electronic structure of metallic systems is fitted to the band structures and total energies obtained from DFT calculations, as a function of volume, for face-centered, body-centered and simple-cubic structures. This TB scheme is also compatible with molecular dynamics. Such parameterization has reproduced many static[28] and dynamic[29, 30] gold properties. In the MD implementation of the TBINS code, the equations of motion of each atom are integrated using the Verlet-algorithm and the temperature is controlled within the Langevin scheme. When performing our TBMD calculations, we only considered the top-and-bottom pulling mechanism

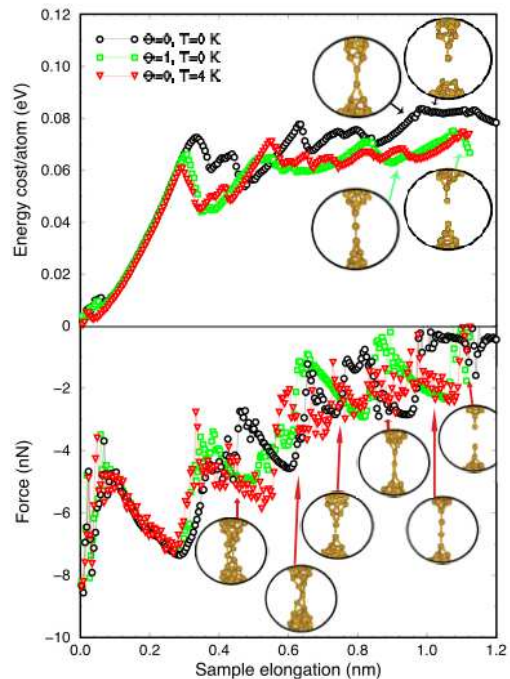


FIG. 3: (a) Energy cost per atom versus sample elongation from the TBMD simulations. Deformation along the [110] and [99 101 2] tensile axes is labeled “ $\theta = 0$ ” and “ $\theta = 1$ ”, respectively, and the simulation temperatures are listed. The insets show the atomic configurations just before and after the NWs break, and the arrows indicate the corresponding elongation distance and tensile direction for  $T=0 \text{ K}$ . (b) Plot of tensile forces as a function of sample elongation. The corresponding configurations for  $T=4 \text{ K}$  are shown in this figure (here we show  $\theta = 0$ , but a similar result is obtained for  $\theta \approx 1$ ).

and stretched the NW in a continuous manner, using stretching velocities of 25 m/s. These velocities are much larger than those used in typical nanocontact experiments, but still small compared to the speed of sound through the material, providing the system with enough time to relax[9, 10, 11, 12, 13, 14, 31]. During the simulations, the atoms between the frozen slabs move and accommodate into new configurations according to the molecular dynamics procedure. The simulation cell is nearly identical to the one used above in the DFT calculations. We considered a time step of 4 fs, and a temperature of 4 K to simulate the experimental conditions of refs.[3, 11]), and 0 K to perform semistatic relaxation calculations akin to those done within the DFT framework. During the elongation process we computed the energy cost per atom as well as the tensile force along the stretching direction.

As before, two tensile axes are considered: parallel to the [110] and a slightly off-axis case (about 1 degree off the [110] direction). Fig. 3a shows the resulting energy cost per atom as a function of the elongation distance of the sample. The circle, triangle and square symbols correspond to the gold NW elongation process for the symmetric ( $T=0 \text{ K}$  and  $T=4\text{K}$ ) and the off-axis ( $T=0$

K) cases, respectively. The insets in this figure depict the corresponding atomic configurations just before and after the NW breaks for the T=0 K case, while the configurations obtained for T=4 K (triangle symbols) are shown in Fig. 3b. When comparing Fig. 1 and Fig. 3a, we note that the energy costs and ultimate elongation distances are very similar to the DFT calculations, and that non-SAC NW breaking again corresponds to the higher energy cost. These results demonstrate the reliability of the TB approximation considered here. Moreover, at T=0 K, a neck containing only two gold atoms forms for the symmetric case, while for the non-symmetric case a chain of three-atoms is formed. For the first case, both bonds below the atom in the neck stretch to accommodate the imposed strain and the chain breaks at this location. The T=0 K TBMD and DFT simulations therefore agree that high-symmetry stretching favors the simultaneous breaking of multiple bonds, while off-symmetry stretching favors SAC formation. On the other hand, at T=4 K, the TBMD calculations predict suspended SACs containing 4 (see Fig. 3b) and 5 atoms (data not shown), independent of the symmetry, thus demonstrating that small thermal fluctuations provide enough symmetry breaking to allow SAC formation.

Fig. 3b shows the tensile forces as a function of sample elongation. As observed experimentally[32], the tensile force increases (becomes more negative) with elongation and decreases when an atom is detached from the thinning gauge section. Also, the force needed to detach

an atom and break the NW is consistent with our DFT calculations and with experiments[11]. For T=4 K, we note that the thermal fluctuations produce a noisier force curve than that observed for T=0 K. These fluctuations allow the system to explore a wider range of configurations in the potential energy surface.

In summary, we found abrupt breaking of the NWs in the completely symmetric case when thermal fluctuations are neglected, and a SAC when the crystal symmetry is broken in the early stages of the NW elongation process. Such crystallographic asymmetry can be induced by stretching the wire along a slightly off-axis direction or by introducing small thermal fluctuations. The observation of the off-axis formation of these chains agrees with experimental results[6], where SAC formation was favored for tensile axes that were not parallel to the main crystal axis. We found that the distance between gold atoms within the chain ranged from 0.26 nm to 0.31 nm, in agreement with the bond distances reported in experiments[3, 6]. These findings represent the first quantum calculations on the formation of suspended SACs when stretching gold NWs along the [110] crystal orientation. Our molecular dynamics simulations show that the static geometrical model considered in ref.[4] to justify the non-formation of gold monatomic chains in the [110] direction is insufficient. Only a detailed description of the kinetics of the nanocontact elongation process can reproduce realistic experimental conditions.

- 
- [1] For a review, see Nanowires, edited by P. A. Serena and N. García, NATO ASI Series E: Applied Sciences (Kluwer, Dordrecht, 1997), Vol. 340.
- [2] H. Ohnishi, Y. Kondo, and K. Takayanagi, *Nature* **395**, 780 (1998).
- [3] A.I. Yanson et al., *Nature* **395**, 783 (1998).
- [4] V. Rodrigues, T. Fuhrer and D. Ugarte, *Phys. Rev. Lett.* **85**, 4124 (2000).
- [5] V. Rodrigues and D. Ugarte, *Eur. Phys. J. D* **16**, 395 (2001).
- [6] Y. Takai et al., *Phys. Rev. Lett.* **87**, 106105 (2001).
- [7] J.A. Torres et al. *Surf. Sci.* **426**, L441 (1999).
- [8] D. Sanchez-Portal et al. *Phys. Rev. Lett.* **83**, 3884 (1999).
- [9] M.R. Sorensen, M. Brandbyge, and K.W. Jacobsen, *Phys. Rev. B* **57**, 3283 (1998).
- [10] S.R. Bahn and K.W. Jacobsen, *Phys. Rev. Lett.* **87**, 266101 (2001).
- [11] G. Rubio-Bollinger et al. *Phys. Rev. Lett.* **87**, 026101 (2001).
- [12] P.Z. Coura et al. *Nanoletters* **4**, 1187 (2004).
- [13] F. Sato et al., *Apply. Phys. A* **81**, 1527 (2005).
- [14] H.S. Park and J.A. Zimmerman, *Phys. Rev. B* **72**, 054106 (2005).
- [15] E.Z. da Silva, A.J.R. da Silva, and A. Fazzio, *Phys. Rev. Lett.* **87**, 256102 (2001).
- [16] E.Z. da Silva et al. *Phys. Rev. B* **69**, 115411 (2004).
- [17] M.J. Mehl and D.A. Papaconstantopoulos, *Phys. Rev. B* **54**, 4519 (1996).
- [18] Commercial software is identified to specify procedures. Such identification does not imply recommendation by the National Institute of Standards and Technology.
- [19] B. Delley, *J. Chem. Phys.* **92**, 508 (1990).
- [20] B. Delley, *J. Chem. Phys.* **113**, 7756 (2000).
- [21] Perdew, Burke and Ernzerhof, *Phys. Rev. Lett.* **77**, 3865 (1996).
- [22] B. Delley, *Phys. Rev. B* **66**, 155125 (2002).
- [23] P.Pulay and G.Fogarasi, *J.Chem.Phys.* **96**, 2856 (1992).
- [24] J.Baker, A.Kessi, and B.Delley, *J. Chem. Phys.* **105**, 192 (1996).
- [25] Among many: P. Jelinek et al., *Phys. Rev. Lett* **96**, 046803 (2006); *Phys. Rev. B* **68**, 085403 (2003).
- [26] F. Picaud, A. Dal Corso, and E. Tosatti, *Surf. Sci.* **532**, 544 (2003).
- [27] L. Rincón and A. Hasmy (unpublished).
- [28] M.I. Haftel et al., *Phys. Rev. B* **70**, 125419 (2004).
- [29] F. Kirchoff et al., *Phys. Rev. B* **63**, 195101 (2001).
- [30] A. Hasmy, L. Rincón, M. Márquez and C.A. González (to be published).
- [31] A. Hasmy, E. Medina, and P. A. Serena, *Phys. Rev. Lett.* **86**, 5574 (2001).
- [32] G. Rubio, N. Agrait, and S. Vieira, *Phys. Rev. Lett.* **76**, 2302 (1996).